

Article

The Influence of Metal Lithium and Alkyl Chain in the Nucleating Agent Lauroyloxy-Substituted Aryl Aluminum Phosphate on the Crystallization and Optical Properties for iPP

Fuhua Lin ^{1,2,3} , Mi Zhang ², Shuangdan Mao ⁴, Jianjun Zhang ², Kezhi Wang ², Jun Luo ⁵, Xinde Chen ³, Bo Wang ^{4,*}  and Yinghui Wei ^{1,*}

¹ School of Materials Science and Engineering, Taiyuan University of Science and Technology, Taiyuan 030024, China

² Shanxi Provincial Institute of Chemical Industry (Co., Ltd.), Jinzhong 030600, China

³ Key Laboratory of Renewable Energy, Guangzhou Institute of Energy Conversion, Chinese Academy of Sciences, Guangzhou 510640, China

⁴ School of Chemical Engineering and Technology, Taiyuan University of Science and Technology, Taiyuan 030024, China

⁵ Guangzhou Fibre Product Testing and Research Institute, Guangzhou 510220, China

* Correspondence: wangbo@tyust.edu.cn (B.W.); weiyinghui@tyust.edu.cn (Y.W.); Tel.: +86-351-6938220 (B.W.)

Abstract: In this work, a kind of aryl phosphate salt nucleating agent (APAl-12C) was synthesized, which was replaced in the hydroxyl group on the aluminum hydroxy bis [2,2'-methylene-bis(4,6-di-tert-butylphenyl) phosphate] (APAl-OH) by lauroyloxy, which could improve the dispersion between the nucleating agent and the iPP matrix and reduce the migration potential of the nucleating agent in the iPP matrix by increasing the molecular weight. The structure of the nucleating agent APAl-12C was analyzed by fourier infrared spectroscopy (FT-IR) and ¹H NMR. The differential scanning calorimeter (DSC) results indicated that the addition of APAl-OH or APAl-12C alone was inferior to the commercial nucleating agent NA-21 (compounds of APAl-OH and Lithium laurate) in terms of the crystallization behavior, which may be due to the importance of metal Li in the crystallization property. Thus, the iPP/A12C-Li composites were prepared with APAl-12C, lithium laurate (lilaurate) and the iPP matrix. The crystallization behavior, morphology, optical and mechanical properties for the iPP/A12C-Li composites were systematically studied and compared with that of the iPP/NA-21 composite. Among the iPP/A12C-Li composites with the addition of 0.5 wt%, APAl-12C/Lilaurate had the fastest crystallization rate and reduced the haze value of the neat iPP from 36.03% to 9.89% without changing the clarity, which was better than that of the iPP/NA-21 composite. This was due to the weakening of the polarity of the APAl-12C after lauroyloxy substitution and better dispersion in the iPP matrix, resulting in a significant improvement in the optical properties.

Keywords: isotactic polypropylene (iPP); aryl phosphate salt; crystallization behavior; optical property; mechanical property



Citation: Lin, F.; Zhang, M.; Mao, S.; Zhang, J.; Wang, K.; Luo, J.; Chen, X.; Wang, B.; Wei, Y. The Influence of Metal Lithium and Alkyl Chain in the Nucleating Agent Lauroyloxy-Substituted Aryl Aluminum Phosphate on the Crystallization and Optical Properties for iPP. *Polymers* **2022**, *14*, 3637. <https://doi.org/10.3390/polym14173637>

Academic Editor:
Nicolas Sbirrazzuoli

Received: 22 July 2022

Accepted: 29 August 2022

Published: 2 September 2022

Publisher's Note: MDPI stays neutral with regard to jurisdictional claims in published maps and institutional affiliations.



Copyright: © 2022 by the authors. Licensee MDPI, Basel, Switzerland. This article is an open access article distributed under the terms and conditions of the Creative Commons Attribution (CC BY) license (<https://creativecommons.org/licenses/by/4.0/>).

1. Introduction

Isotactic polypropylene (iPP) has one of the best heat resistances among general resins and is widely used in the chemical industry, construction, automobile manufacturing and packaging materials because of its low density, easy processing, impact resistance and bending resistance [1–3]. Despite the outstanding advantages, the processing and application properties of iPP are directly affected by its crystallization speed, morphology and spherulite size, which restricts the application to a certain extent [4–6]. At present, the most simple and efficient modification method is adding the nucleating agent into the iPP matrix.

Aryl phosphate salts (APs) are a kind of important nucleating agent in the application of iPP modification [7]. The main commercial brands are NA-11, NA-21, TMP-6, etc. NA-21

is the third generation nucleating agent of APs, which has the advantages of stiffness enhancement, high transmittance, good thermal stability and no peculiar smell during processing. Especially for the optical performance of iPP, NA-21 is much superior to that of NA-11 [8].

As we all know, NA-21 is a kind of compound nucleating agent where the major constituent is aluminum hydroxy bis [2,2'-methylene-bis(4,6-di-tert-butylphenyl) phosphate] (APAl-OH, as shown in Figure 1), and the ligand is an alkyl carboxylic salt [9,10]. Several researchers have theoretically investigated that adding one component alone does not significantly improve the crystallization and the optical performance of iPP [11,12]. Kimura et al. [13] proposed, for the first time, that the synergistic effect of APAl-OH and lithium laurate can reduce the haze of PP from 32% to 5%. As a kind of additive nucleating agent, NA-21 is difficult to disperse in the iPP system because of the presence of strong polar phosphate compounds in its components [14].

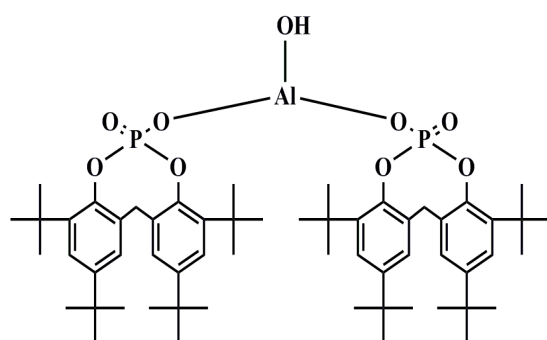


Figure 1. The chemical structure of APAl-OH.

At present, many studies have been devoted to improving the dispersion of the APs nucleating agents in the iPP matrix [15–17]. Li et al. pointed out that the NA-11 could be dispersed to the nanoscale by supercritical carbon dioxide (scCO₂). The crystallization rate and mechanical properties of the PP composites with NA-11 dispersed by scCO₂ were higher than those of untreated PP, while the trend of the haze and the spherulite size was just the opposite [18]. It has been proven that solvents can also promote the dispersion of nucleating agents [19]. The ethanol was chosen as a solvent to prepare micro emulsion lotion of the NA-11 and sodium benzoate composite nucleating agent. The size of the dispersed phase in PP is smaller, and the stiffness of the PP is increased obviously [20]. Meng et al. increased the dispersion of the NA-11 in the iPP by adding zeolite containing hydrogen bonds, accelerating the crystallization rate and improving the tensile strength and the flexural modulus [21]. These studies have suggested that reducing the size or dispersion of the nucleating agents by physical addition can improve the nucleation efficiency. However, the dispersion of the nucleating agent cannot be fundamentally solved, and the introduction of other substances may be affected by the nucleation ability of polymers [22]. In response to the problems, some researchers have theoretically investigated the modification of groups for the structure of the nucleating agents. Zhang et al. modified the glycerol ester onto a phosphate ester. The results indicated that the derivative made the crystallization temperature increase by 11 °C for iPP and the mechanical properties were significantly improved [23]. Long et al. introduced amino functional groups into phosphate ester to prepare a low melting point nucleating agent. Compared with the NA-11, the derivative particles were evenly dispersed in the iPP matrix and their compatibility with the iPP matrix was better than that of the NA-11 [24]. Despite the recent progress reviewed in modified NA-11, there are very few studies on the group modification of NA-21.

In this study, a new nucleating agent, APAl-12C, was synthesized by substituting alkylation for a hydroxyl group of APAl-OH. The primary goal of this research was to discuss the nucleation activities of the APAl-12C, NA-21 and APAl-12C/Lilaurate, focusing on their crystallization behavior and application properties in iPP, especially their optical

and mechanical properties. Moreover, the increase in molecular weight of the nucleating agent has an important influence on reducing the migration potential in the iPP matrix, thereby lowering the impact on the environment. The nucleation behavior was preliminarily explored by a polarizing microscope (POM) and differential scanning calorimetry (DSC). It was expected to explore the role of the alkyl carboxylic acid functional group and Li metal in the nucleation process.

2. Materials and Methods

2.1. Materials

Isotactic polypropylene (K1012, Isotacticity: 97%, M_w : 80,000–150,000) with a melt flow of 12 g/10 min was received from Sinopec Beijing Yanshan Company (Beijing, China). Aluminum isopropoxide, lauric acid and lithium laurate (lilaurate) were purchased from Shanghai McLean Biochemical Technology, China (Co., Ltd.). 2,2'-methylene bis(4,6-di-tert-butyl phenoxy). Phosphate and NA-21 nucleating agent were provided by Shanxi Provincial Institute of Chemical Industry, Jinzhong, China (Co., Ltd.). Toluene was provided from Shanghai Macklin Biochemical, Shanghai, China (Co., Ltd.). All reagents were all of analytical grade.

2.2. Synthesis of Nucleating Agent APAl-12C

The APAl-12C was synthesized as depicted in Figure 2. The addition of 2,2'-methylene bis(4,6-di-tert-butyl phenoxy) phosphate, aluminum isopropoxide and toluene to the reaction flask was followed by stirring and heating for 2 h. Then lauric acid was added to the mixture and maintained for 1 h. The nucleating agent APAl-12C was collected and washed three times using deionized water, and then dried in an oven at 105 °C for 24 h.

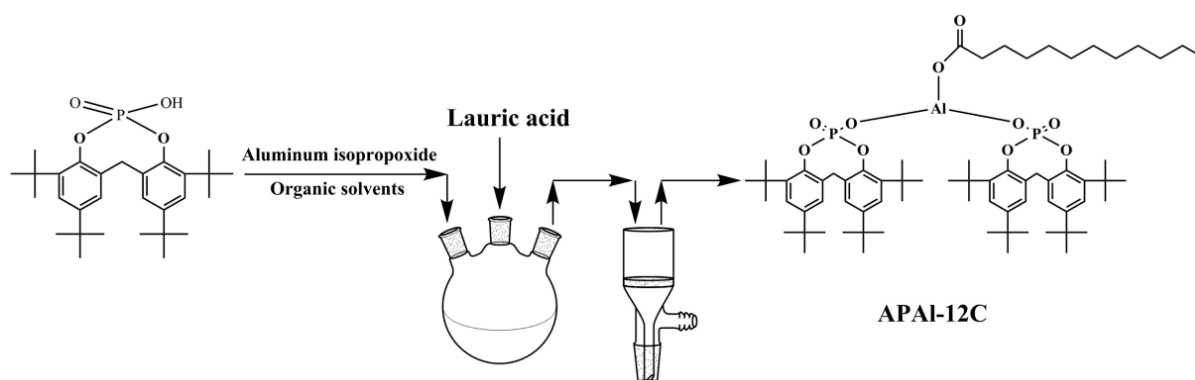


Figure 2. The synthesis of the APAl-12C.

2.3. Preparation of the iPP Composites

The iPP composites were mixed together with different nucleating agents and extruded from a corotating twin-screw extruder. The barrel temperatures were maintained at 175, 180, 185 and 200 °C from the hopper to the mold, and the screw speed was set at 300 r/min. After pelletizing and drying, the extruded iPP composites were dried at above 100 °C for 12 h. The iPP composites with 0.3 wt%, APAl-OH, APAl-12C and NA-21, were prepared and abbreviated as iPP/AOH, iPP/A12C and iPP/NA-21, respectively.

2.4. Characterization

The Fourier transform infrared spectra (FT-IR) was recorded in the range of 4000–600 cm^{-1} using an FT-IR spectrophotometer (Perkin Elmer, Waltham, MA, USA) with the KBr pellet technique.

The nuclear magnetic resonance hydrogen spectrum (^1H NMR) was recorded using a nuclear magnetic resonance spectrometer (Bruker Avance, Karlsruhe, Germany), operating at a frequency of 500 MHz for protons at room temperature. Deuterated methanol was used as the solvent to prepare solutions of 5 $w/v\%$ and the sweep width was 6 kHz.

The thermogravimetric analysis (TGA) of the samples was carried out by a TGA 1 (Mettler Toledo, Zurich, Switzerland) under a nitrogen flow rate of 60 mL/min from 25 to 800 °C with a heating rate of 10 °C/min.

The differential scanning calorimeter (DSC) was employed to observe the crystallization behavior of iPP composites by a DSC 1 (Mettler Toledo) under a nitrogen atmosphere. The conditions for the non-isothermal crystallization behavior of the iPP composites were as follows. The samples were first heated from 25 to 210 °C with a heating rate of 20 °C/min and maintained for 5 min to remove the thermal history. Then, the samples were cooled to 25 °C with a cooling rate of 10 °C/min. After cooling to 25 °C, the samples were reheated to 210 °C at a rate of 10 °C/min. The conditions for the isothermal crystallization behavior of the iPP composites were as follows. The samples were heated from 25 to 210 °C with a heating rate of 20 °C/min and maintained for 5 min to erase the thermal history. Then, the samples were cooled to 128 °C at a rate of 50 °C/min and kept at 128 °C for 1 h.

The crystallization morphology of the iPP composites was studied by a polarized optical microscope (POM, Leica DM 2700, Wetzlar, Germany) equipped with a hot-stage (Linkam THMS 600, Salfords, UK). The samples were heated at 230 °C for 5 min to erase any traces of crystals, and then rapidly cooled to 120 °C. The samples were kept at 120 °C until the crystallization process was completed.

The tensile strength test was carried out using a universal testing machine (M10, Instron, Norwood, MA, USA) with a crosshead speed of 5 mm/min, according to the GB/T1040.2-2006 standard, at a temperature of 25 ± 2 °C. The flexural modulus test was also carried out with the universal testing machine using a three-point bending test mode, according to the GB/T 9341-2008 standard, at a temperature of 25 ± 2 °C. The impact strength was carried out using an impact testing machine (GT-7045-HML, Gaotie, Taiwan, China) with a crosshead speed of 5 mm/min, according to the GB/T 1843-2008 standard, at a temperature of 25 ± 2 °C. At least five times for each sample were tested to obtain an averaged value with standard deviation.

The haze and clarity values of the iPP composites were tested using a WGT-2S test instrument (Shengguang, China).

The dispersion of the nucleating agents in the iPP matrix was characterized by a scanning electron microscope (SEM, JSM-6700F, JEOL, Tokyo, Japan). The test specimens were fractured under liquid nitrogen conditions until a smooth surface was obtained.

3. Results and Discussion

3.1. Characterization of the Nucleating Agent APAl-12C

The APAl-12C is characterized by FT-IR, ¹H NMR, DSC and TG spectroscopy, respectively. The structure of the nucleating agent APAl-12C is tested by FT-IR spectra in Figure 3a. The stretching vibration peaks of $-\text{CH}_2-$ and $\text{C}=\text{O}$ are detected at about 2917 cm^{-1} and 1590 cm^{-1} , which are attributed to the characteristic peaks of lauroyloxy [25]. Moreover, a strong peak at approximately 1476 cm^{-1} could be assigned to the benzene ring stretching vibration [26]. The peaks in the range of 1004 and 944 cm^{-1} are attributed to the stretching vibrations of $\text{C}-\text{O}-\text{P}$ coming from 2,2'-methylene bis(4,6-di-tert-butyl phenoxy) phosphate [27]. In addition, the new peak centered at 1104 cm^{-1} corresponded to the stretching modes of the $\text{P}-\text{O}-\text{Al}$ group from the synthesis reaction for the nucleating agent APAl-12C [28]. The FTIR shows the characteristic peaks of both lauric acid and 2,2'-methylene bis(4,6-di-tert-butyl phenoxy) phosphate, which was corroborated by the successful synthesis of the nucleating agent, APAl-12C. In order to further confirm the structure of the APAl-12C nucleating agent, the chemical shifts of hydrogen atoms at different positions in the molecular structure are analyzed by ¹H NMR in Figure 3b. The protons of the benzene ring appear at 7.28 ppm and 7.33 ppm (" $1&2''\text{C}-\text{H}$ "), whereas the three methyl groups on tert butyl were adjacent to the benzene ring and appear at 1.46 ppm and at 1.31 ppm (" $3''$ " and " $4''-\text{CH}_3$ ") [29,30]. The chemical shift of methylene connecting the two benzene rings appeared at 3.81 ppm (" $5''-\text{CH}_2$ "). The methylene, which was adjacent to the carbon of the ester group, appeared at 2.30 ppm (" $6''-\text{CH}_2$ "), and there were three

splitting peaks in this peak, which related to its connection with another methylene [31]. The band of alkylic R–H (δ H: 0.60–1.80 ppm) shows maxima at 0.9 ppm from terminal methyl hydrogens C–CH₃ (“16”–CH₃) and 1.3 ppm from polymethylene chains –(CH₂)_n– (“8–15”–CH₂) [32]. The above description of the chemical shifts for APAl-12C is consistent with the reported literature. Therefore, the above-mentioned results of FT-IR and ¹H NMR are in line with the successful synthesis of the nucleating agent APAl-12C.

As we all know, the thermostability of the nucleating agents is very important for commercial application [33]. The melting point of the synthetic APAl-12C is analyzed in Figure 3c. It can be seen from the DSC curves that there is no melting peak at 50.78 °C of APAl-12C compared with lauric acid. There is also no endothermic or exothermic process range from 25 to 250 °C in the APAl-12C curve. As shown in Figure 3d, in the TGA curve of the APAl-12C, the initial degradation temperature (defined as the temperature where 5% weight loss occurred [34]) is about 256 °C, which is higher than the 235 °C reported as the initial decomposition temperature of pure iPP [35]. Therefore, combined with the curves of DSC and TGA, it can be concluded that the APAl-12C nucleating agent has a thermostability below 250 °C, which will not change its structure during the processing of iPP.

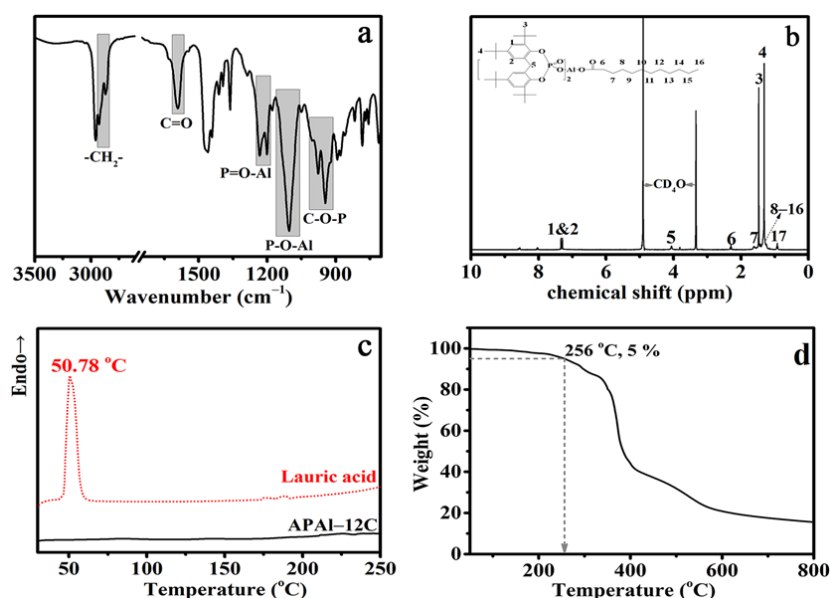


Figure 3. FT-IR (a), ¹H NMR (b), DSC (c) and TGA (d) spectroscopy of the APAl-12C nucleating agent.

3.2. Crystallization Behavior of the iPP Composites

The non-isothermal crystallization process is commonly used to study the nucleation ability of different nucleating agents for polymers [36]. The overall crystallization behavior of the iPP composites carried over in an N₂ atmosphere, as shown in Figure 4. The neat iPP has a single crystallization peak at about 106.67 °C. The value of the crystallization peak temperatures ($T_{c,p}$), both iPP/A12C and iPP/AOH, exceeded that of pure iPP, which revealed that the presence of APAl-OH or APAl-12C can shift the $T_{c,p}$ of iPP towards a higher temperature regime slowly, promoting the iPP composites' crystallization in advance during processing. It is worth mentioning that under the concentration of 0.3 wt% APAl-12C, the value of $T_{c,p}$ for the iPP/A12C composite is 114.68 °C higher than 110.09 °C for the iPP/AOH composite with 0.3 wt% APAl-OH, suggesting that the nucleating ability of the APAl-12C is superior to APAl-OH, which is mainly ascribed to the decrease in polarity between APAl-12C and the iPP matrix because of the replacement of the hydroxyl group on the APAl-OH structure with lauroyloxy. On the other hand, the nucleation ability of the iPP/A12C composite is inferior to that of the iPP/NA-21 composite, where the value of $T_{c,p}$

for the iPP/NA-21 composite is 2.84 °C higher than the iPP/AOH composite at the same concentration of the nucleating agents. The DSC result shows that the direct substitution of lauryloxy structure can improve the nucleation ability of iPP to a certain extent, but it is far less than NA-21, which may be due to the role of metal Li in the NA-21 component, which is irreplaceable in terms of the crystallization behavior.

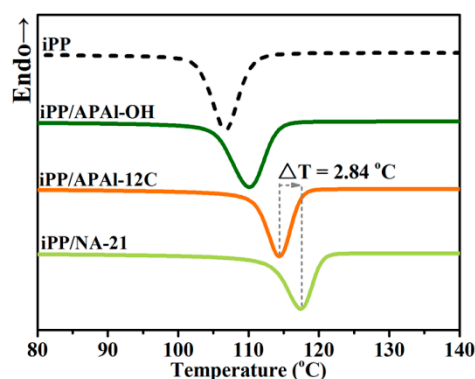


Figure 4. The DSC curves for the iPP composites.

On the basis of this view that metal Li may be the key factor in the nucleation ability of iPP, we make the speculation that if metal Li is introduced into APAI-12C, will the crystallization property of iPP be improved to the equivalent of that of NA-21? So, the iPP/A12C-Li composites were prepared with the APAI-12C and lilaurate according to the formula in Table 1.

Table 1. The formula of the iPP/A12C-Li composites.

Samples	iPP/wt%	APAI-12C/Lilaurate (6:4, Mass Ratio)/wt%
iPP-1	99.95	0.05
iPP-2	99.90	0.10
iPP-3	99.70	0.30
iPP-4	99.50	0.50
iPP/NA-21	99.50	0.50

3.3. The Crystallization Behavior for the iPP/A12C-Li Composites

The overall non-isothermal crystallization behavior for the iPP/A12C-Li composites is carried over in an N₂ atmosphere, as shown in Figure 5a, and the corresponding $T_{c,p}$ values are presented in Figure 5b. The $T_{c,p}$ for the iPP-3 composite with the concentration of 0.3 wt% APAI-12C/Lilaurate is increased to 117.86 °C compared with 114.68 °C of the iPP/A12C composite with 0.3 wt% of APAI-12C, further verifying that the presence of metal Li has an important influence on the nucleation ability of iPP. Meanwhile, with the increase in APAI-12C/Lilaurate concentration, the $T_{c,p}$ for the iPP/A12C-Li composites gradually moved towards higher temperatures. While adding 0.5 wt% APAI-12C/lilaurate, the value of $T_{c,p}$ for the iPP-4 composite reached 118.67 °C, which is 12 °C higher than pure iPP, illustrating the high synergistic nucleation efficiency between APAI-12C and lilaurate. Apart from this, there is no obvious difference between the APAI-12C/lilaurate and NA-21 as the aspect of $T_{c,p}$, which can be verified that the crystallization property of the iPP composites with the APAI-12C/lilaurate is equivalent to that of the NA-21.

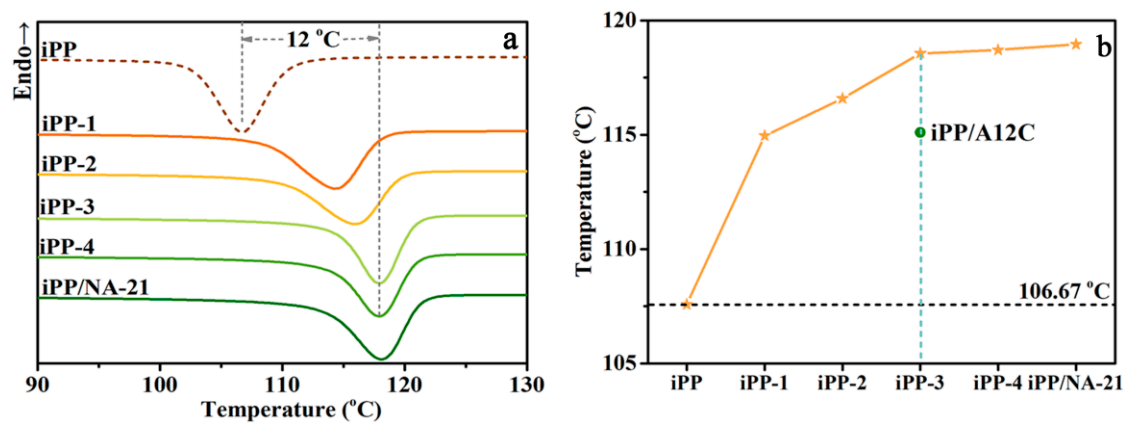


Figure 5. The non-isothermal crystallization curves (a) and the related $T_{c,p}$ (b) for the iPP/A12C-Li composites under a cooling rate of $10\text{ }^{\circ}\text{C}/\text{min}$.

In order to study the synergistic nucleation efficiency between APAI-12C and lilaurate on iPP, the isothermal crystallization behavior for the iPP/A12C-Li composites was investigated under a crystallization temperature of $128\text{ }^{\circ}\text{C}$, and the corresponding curves are presented in Figure 6. The effect of APAI-12C/Lilaurate concentration on the crystallization rate can be observed clearly and the addition of only 0.05 wt% APAI-12C/lilaurate can shorten the crystallization time from nearly 30 min to about 12 min. As the APAI-12C/lilaurate concentration increased, the crystallization peak became very narrow and sharp, which indicates that the crystallization time is shorter and the crystallization rate has increased rapidly. In addition, it can be seen from Figure 6 that the iPP-4 composite with the addition of 0.5 wt% APAI-12C/lilaurate has almost the same crystallization time compared with that of the iPP/NA-21 composite with 0.5 wt% NA-21, which further proves that the crystallization effect of APAI-12C/lilaurate on the iPP is equivalent to that of NA-21.

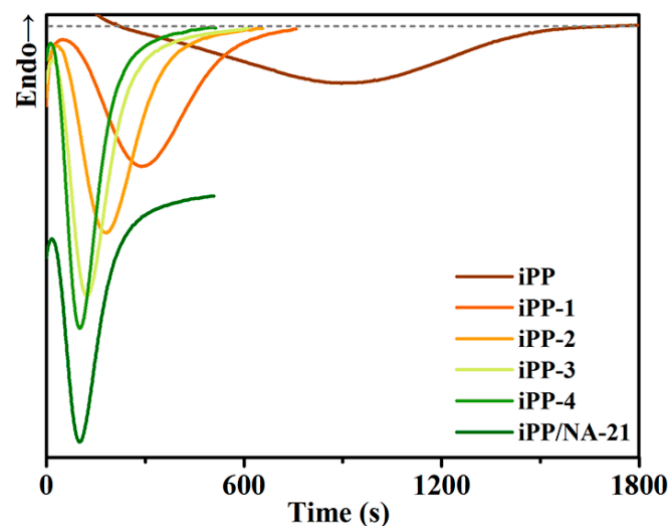


Figure 6. The isothermal crystallization curves for the iPP/A12C-Li composites.

In order to further evaluate the nucleation and crystal growth of the iPP/A12C-Li composites, the classical Avrami model can be used to analyze the crystallization kinetics as in the following, Equation (1) [37,38]:

$$1 - X_t = \exp(-Kt^n) \quad (1)$$

where the Avrami exponent n is relative to the nucleation mechanism and growth manner of the crystal, the crystallization rate constant K depends on the crystallization temperature

and contains both nucleation and growth contributions, and the relative crystallinity (X_t) is calculated with Equation (2) [39] at a different crystallization time.

The X_t is calculated by the integration of the crystallization peaks at different crystallization times, Equation (2):

$$X_t = \frac{X_t(t)}{X_t(\infty)} = \frac{\int_0^t \left(\frac{dH(t)}{dt} \right) dt}{\int_0^\infty \left(\frac{dH(t)}{dt} \right) dt} \quad (2)$$

where $(dH(t)/dt)$ represents the heat flow. $X_t(t)$ and $X_t(\infty)$ denote the absolute crystallinity at time (t) and at the termination of the crystallization process, respectively.

The Avrami equation can be written as follows (3):

$$\ln[-\ln(1 - X_t)] = n \ln t + \ln K \quad (3)$$

The values of semicrystalline time ($t_{1/2}$) are generally used to describe the crystallization rate of iPP. The $t_{1/2}^a$ calculated from the Avrami model can be calculated as follows (4) [40]:

$$t_{1/2} = \left(\frac{\ln 2}{K} \right)^{1/n} \quad (4)$$

The nucleation effect of APAI-12C/lilaurate is evaluated more evidently by the relative crystallinity curves reported in Figure 7a. It can be seen that all the curves show the S-type characteristic of the polymer material crystals [41]. The relation of $\ln[-\ln(1 - X_t)]$ versus $\ln t$ of the iPP/A12C-Li composites is illustrated in Figure 7b, and the calculated values of n and K are summarized in Table 2. The value of n for neat iPP is about 3.60, which is close to the value of 3.70 reported in the literature [42], suggesting that the iPP crystallization mechanism is homogeneous nucleation and three-dimensional spherulite growth. While adding a small amount of APAI-12C/lilaurate, the value of n is close to that of neat iPP, indicating that the low content of APAI-12C/lilaurate will not change the spherulite growth patterns of iPP. However, with the increased addition of APAI-12C/lilaurate, the n value gradually approaches 3 and the spherulite growth patterns transform from homogeneous nucleation to heterogeneous nucleation. Moreover, the crystallization rate constant's K increases with the addition of APAI-12C/lilaurate, revealing that the increasing of APAI-12C/lilaurate content is beneficial to improving the crystallization rate under the temperature of 128 °C. As we all know, the shorter the $t_{1/2}$ value, the faster the crystallization rate [43]. The value of $t_{1/2}^a$ is related to the n and K parameters, and the calculated values are summarized in Table 2. Meanwhile, the $t_{1/2}^b$ determined from Figure 7a is listed in Table 2, too. There is no significant difference between $t_{1/2}^a$ and $t_{1/2}^b$, which demonstrates further that the Avrami equation is quite successful for analyzing the experimental data of the isothermal crystallization kinetics for the iPP/A12C-Li composites. With the increasing content of APAI-12C/lilaurate, the change trend of $t_{1/2}$ is the same as that of the n value, and the addition of APAI-12C/lilaurate can shorten $t_{1/2}$ of iPP obviously. Under the crystallization temperature of 128 °C, the $t_{1/2}$ of neat iPP is about 901.8 s, which is longer than that of the iPP composites with APAI-12C/lilaurate. With the increasing content of APAI-12C/lilaurate, the value $t_{1/2}$ decreases sharply. When the addition amount is 0.5 wt%, the $t_{1/2}$ is the shortest and reaches 112.8 s, which is more than 7 times shorter than that of pure iPP, indicating better nucleation efficiency and a faster crystallization rate. It can be ascribed to the incorporation of APAI-12C/lilaurate in iPP, which promotes the increase of nucleation sites and the free energy barrier of nucleation is reduced because of the existing epitaxial crystallization, thereby resulting in an increase in the nucleation rate. The $t_{1/2}$ value of the iPP composite with 0.5 wt% APAI-12C/lilaurate is the same as that of the iPP composite with 0.5 wt% NA-21, which indicates that the crystallization rate of the APAI-12C/lilaurate is equal to that of NA-21, which further suggests that the crystallization rate of APAI-12C/lilaurate is equal to that of NA-21.

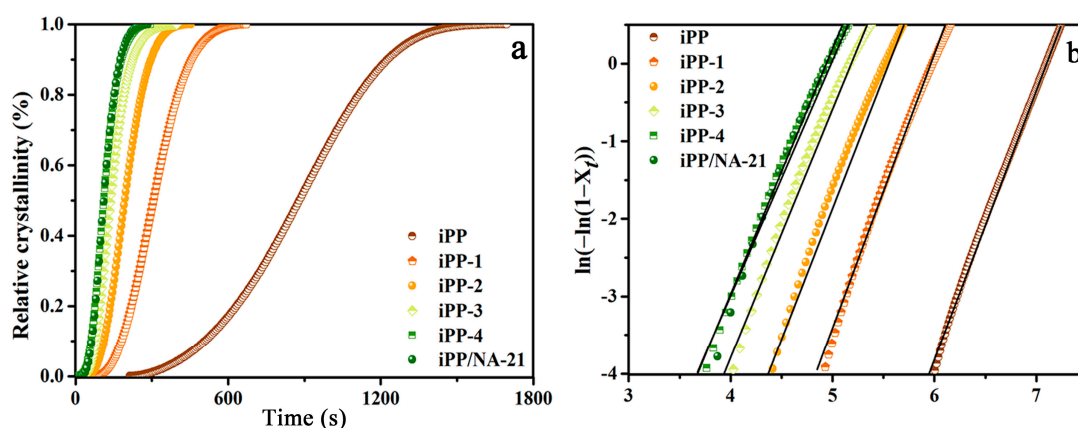


Figure 7. The relative crystallinity curves (a) and the relation of $\ln[-\ln(1 - X_t)]$ versus $\ln t$ (b) for the iPP/A12C-Li composites.

Table 2. The isothermal crystallization parameters for the iPP/A12C-Li composites.

Samples	T ($^{\circ}\text{C}$)	n	K	$t_{1/2}^a$ (s)	$t_{1/2}^b$ (s)
iPP	128	3.60	0.00004	900.6	901.8
iPP-1		3.70	0.00160	309.6	307.2
iPP-2		3.52	0.01045	197.4	195.6
iPP-3		3.38	0.03802	141.6	139.2
iPP-4		3.27	0.08278	114.6	112.8
iPP/NA-21		3.48	0.07364	114.6	112.2

^a Calculated from Avrami parameters. ^b Determined from Figure 7a.

In summary, we can draw the conclusion that the replacement of the hydroxyl group on the APAI-OH structure with lauryloxy can improve the crystallization ability of iPP to some extent, but the crystallization ability of the iPP/APAI-12C is far inferior to that of iPP/NA-21, which further proves that the direct substitution of the alkyl carboxylic structure cannot achieve the synergistic nucleation of APAI-OH and lithium alkyl carboxylate, and the role of metal Li is irreplaceable in terms of the crystallization behavior of iPP.

3.4. The Crystal Morphology for the iPP/A12C-Li Composites

POM is the most intuitive tool to observe the nucleation and the crystal growth process of the crystalline polymer. Figure 8 exhibits the POM micrographs for the iPP/A12C-Li composites under the isothermal crystallization temperature of 128 $^{\circ}\text{C}$. Obviously, the neat iPP has a few nuclei and grows in a three-dimensional mode with large spherulites and clear boundaries [44]. The presence of 0.05 wt% APAI-12C/Lilaurate effectively increases the number of nuclei, significantly reduces the grain size and the growth mode is the same as that of the neat iPP. However, when the addition amount is 0.5 wt%, both APAI-12C/lilaurate and NA-21, a large number of nuclei are induced within a short time, accelerating the crystallization of iPP, where the spherulites overlap each other and hence become much smaller than those in pristine iPP. This could be attributed to the presence of the APAI-12C/lilaurate nucleating agent, exhibiting an excellent nucleation effect for the iPP [45].

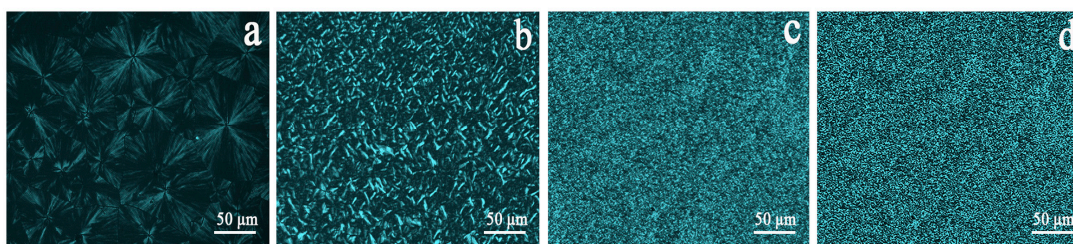


Figure 8. POM micrographs for the iPP/A12C-Li composites under isothermal crystallization temperature of 128 °C: (a) iPP; (b) iPP-1; (c) iPP-3; (d) iPP/NA-21.

3.5. The Optical Property for the iPP/A12C-Li Composites

Thus, we measured the clarity and haze values of the iPP/A12C-Li composites with different concentrations of APAI-12C/lilaurate, and the results are presented in Figure 9. It is fortunate that the addition of APAI-12C/lilaurate will not lead to a change in clarity value. However, the haze value reduces rapidly along with the increase in the concentration of APAI-12C/lilaurate, which is consistent with the crystallization temperature results of the iPP/A12C-Li composites. The haze value is decreased to less than 15% under the concentration of 0.3 wt% APAI-12C/lilaurate. When adding 0.5 wt% APAI-12C/lilaurate to the iPP matrix, the haze value of the iPP composite is only 9.89%, which is lower than that of NA-21 at the same concentration. From this, we can draw the conclusion that the substitution of the lauroyloxy group reduces the overall polarity of APAI-12C/lilaurate, making the dispersion of APAI-12C/lilaurate in the iPP more uniform than NA-21, thus improving the optical properties of the iPP [46]. This conjecture can also be verified from the POM images of the iPP/A12C-Li composite and the iPP/NA-21 composite. As presented in Figure 10, the rod-shaped nuclei in the iPP matrix could be observed clearly. This could be attributed to the heterogeneous nucleation of the nucleating agent. Moreover, the APAI-12C/Lilaurate nuclei disperse uniformly in the iPP matrix. However, the nuclei of the NA-21 are prone to aggregation, indicating that the dispersion of NA-21 in the iPP matrix is underdeveloped, which is further explained by SEM of the iPP composites.

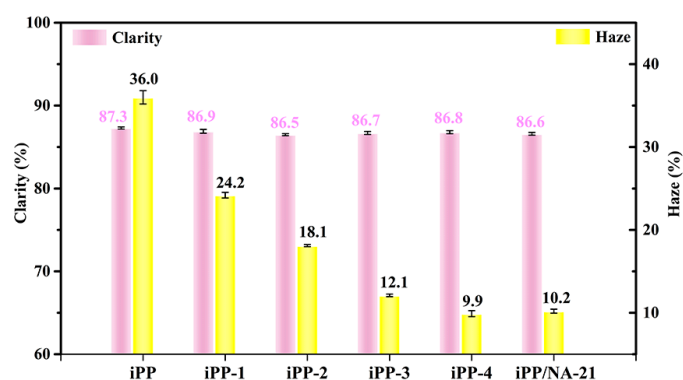


Figure 9. The optical performances for the iPP/A12C-Li composites.

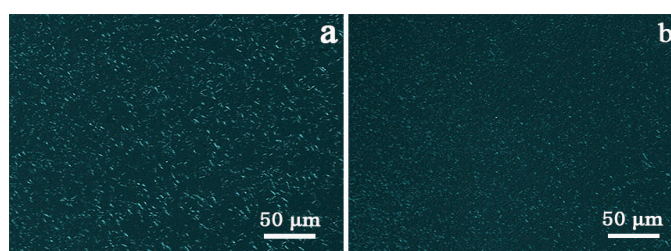


Figure 10. The POM micrographs for iPP-3 (a) and iPP/NA-21 (b) composites under isothermal crystallization at 135 °C for 5 min.

3.6. The Dispersion of Nucleating Agents for the iPP/A12C-Li Composites

The interfacial interaction and dispersion of the nucleating agent in polymers has a great influence on application properties, such as crystallization and mechanical and optical properties [47]. In order to compare the dispersion of APAI-12C/lilaurate and NA-21 in the iPP matrix, the fracture surface of the iPP/A12C-Li composites is observed using SEM. As described in Figure 11a, the NA-21 particles are dispersed unevenly in the iPP matrix. Moreover, some agglomeration and gaps can be observed, which indicates the poor interfacial interaction between NA-21 and iPP. On the contrary, there are no obvious visible particles in the iPP-3 composite with 0.5 wt% APAI-12C/lilaurate in Figure 11b, which suggests that APAI-12C/lilaurate is uniformly dispersed in the iPP matrix. The SEM result demonstrates that APAI-12C/lilaurate has better compatibility with the iPP than that of the NA-21, which owes to the fact that the replacement of the lauroxyloxy for hydroxyl enhances the interfacial interaction between the APAI-12C/lilaurate and the iPP matrix, enhancing the application properties of the iPP in turn. The SEM results are consistent with the conclusion of the POM.

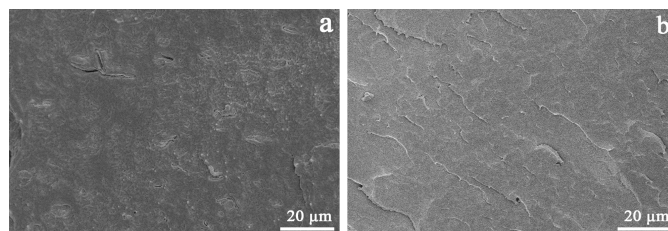


Figure 11. The SEM micrographs of the iPP/NA-21 composite (a) and iPP-3 composite (b).

3.7. The Mechanical Property for the iPP/A12C-Li Composites

The study of the effects of APAI-12C/lilaurate with different contents on the mechanical properties of the iPP has an instructive significance for commercial application. Figure 12 shows the mechanical performances of the iPP/A12C-Li composites, and the full outcomes are summarized in Table 3. During the addition of APAI-12C/lilaurate, the flexural modulus and tensile strength of the iPP composites were enhanced gradually. When the addition amount reached 0.5 wt%, both the flexural modulus and tensile strength reached their maximum values, which were increased by 16.3% and 10.6%, respectively. The tensile strength and the flexural modulus values demonstrate an identical tendency. The toughness and rigidity generally displayed the opposite tendency. The addition of the APAI-12C/lilaurate enhanced the impact strength of the iPP. When the addition amount was 0.05 wt%, the impact strength rose most significantly, which enhanced by 33.2%. However, the change in the impact strength is the opposite to the change in addition amount of APAI-12C/lilaurate. With the increase in addition amounts of APAI-12C/lilaurate, the impact strength decreased gradually, and still increased by about 19.2% when the addition amount was 0.5 wt%. Furthermore, there are no significant differences observed in the tensile strength, flexural modulus and impact strength results with the nucleating agent of APAI-12C/lilaurate and NA-21 in the iPP. It can be noted that the incorporation of APAI-12C/lilaurate and NA-21 has a considerable influence on the mechanical properties and has an exceptional equilibrium on the rigidity and toughness.

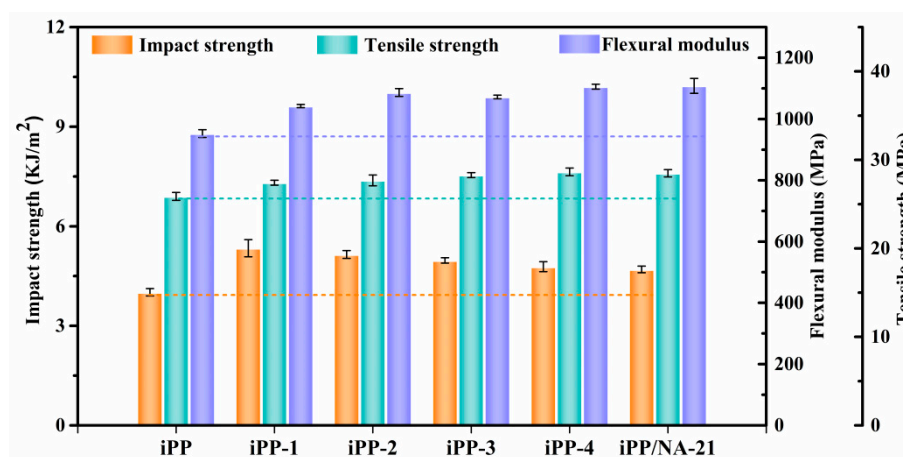


Figure 12. The mechanical properties for the iPP/A12C-Li composites.

Table 3. The mechanical performances for the iPP/A12C-Li composites.

Sample	Impact Strength (KJ/m ²)	Tensile Strength (MPa)	Flexural Modulus (MPa)
iPP	4.0 ± 0.11	25.9 ± 0.45	952.7 ± 12.48
iPP-1	5.3 ± 0.26	27.4 ± 0.28	1042.6 ± 5.32
iPP-2	5.2 ± 0.12	27.7 ± 0.61	1086.6 ± 12.83
iPP-3	4.0 ± 0.08	28.3 ± 0.28	1072.1 ± 5.89
iPP-4	4.8 ± 0.15	28.7 ± 0.43	1105.8 ± 8.03
iPP/NA-21	4.7 ± 0.10	28.5 ± 0.41	1108.5 ± 24.29

4. Conclusions

The APAI-12C nucleating agent was synthesized by lauroyloxy, which substituted the hydroxyl in APAI-OH. The nucleation ability of the APAI-12C for iPP was analyzed by DSC and POM. The $T_{c,p}$ of the iPP/APAI-12C composites is significantly lower than that of iPP/NA-21 (NA-21 is compounded with APAI-OH and lithium alkylate), which can be explained by the fact that the direct substitution of the alkyl carboxylic structure cannot achieve synergistic nucleation of the APAI-OH and lithium alkyl carboxylate for iPP. When lithium laurate and APAI-12C are added into the iPP matrix, it is found that the $T_{c,p}$ for iPP is greatly improved by the APAI-12C/lilaurate nucleating agent, which is basically equivalent to that of the NA-21 under the same concentration. This result also proves that Li metal is an indispensable component in terms of crystallization performance. With the increase in the APAI-12C/lilaurate amounts, the crystal morphology of the iPP/A12C-Li composites changed from three-dimensional spherulite to two-dimensional growth mode, and the n value of 0.5 wt% APAI-12C/lilaurate was close to 2. The tensile strength, flexural modulus and impact strength of the iPP/A12C-Li composites with 0.5 wt% of APAI-12C/lilaurate increased by 10%, 16% and 19%, respectively. The presence of APAI-12C/lilaurate not only increases the rigidity but also improves the toughness of iPP, realizing the balance of rigidity and toughness of iPP, which is due to the weakening of the polarity of APAI-12C after lauroyloxy substitution and better dispersion in the iPP matrix, resulting in significant improvement in the mechanical properties. Moreover, the increase in molecular weight of the nucleating agent had an important influence on reducing the migration potential in the iPP matrix, lowering the impact on the environment.

Author Contributions: Author Contributions: Conceptualization, F.L., J.L. and M.Z.; methodology, J.Z. and K.W., X.C.; formal analysis, S.M.; investigation, F.L.; resources, B.W.; data curation, S.M.; writing-original draft preparation, F.L.; writing-review and editing, B.W.; funding acquisition, F.L., B.W. and Y.W. All authors have read and agreed to the published version of the manuscript.

Funding: This research was funded by the Key Technologies R&D Program of Shanxi (202102040201004), the Scientific and Technological Innovation Programs of Higher Education Institutions in Shanxi (2021L315), the Excellent Innovation Project of Shanxi Postgraduates (2021Y685) and the CAS Key Laboratory of Renewable Energy (E129kf0601).

Institutional Review Board Statement: Not applicable.

Informed Consent Statement: Not applicable.

Data Availability Statement: Not applicable.

Conflicts of Interest: The authors declare no conflict of interest.

References

1. Zhang, L.; Wu, W.; Teng, C.; Meng, S. Mechanical properties and space charge behavior of thermally aged polypropylene/elastomer blends. *J. Electrostat.* **2022**, *115*, 103673. [[CrossRef](#)]
2. Odarchenko, Y.; Rosenthal, M.; Hernandez, J.J.; Doblas, D.; Di Cola, E.; Soloviev, M.; Ivanov, D.A. Assessing fast structure formation processes in isotactic polypropylene with a combination of nanofocus X-ray diffraction and in situ nanocalorimetry. *Nanomaterials* **2021**, *11*, 2652. [[CrossRef](#)] [[PubMed](#)]
3. Horváth, F.; Bihari, L.; Bodrogi, D.; Gombár, T.; Hilt, B.; Keszei, B.; Menyhárd, A. Effect of N, N'-Dicyclohexyldicarboxamide homologues on the crystallization and properties of isotactic polypropylene. *ACS. Omega* **2021**, *6*, 9053–9065. [[CrossRef](#)] [[PubMed](#)]
4. Zhang, X.; Zhao, S.; Kuo, S.W.; Chen, W.C.; Xin, Z. An effective nucleating agent for isotactic polypropylene (iPP): Zinc bis-(nadic anhydride) double-decker silsesquioxanes. *Polymer* **2021**, *220*, 123574. [[CrossRef](#)]
5. Yue, Y.; Wang, X.; Feng, J. Concentration effect of a bis-amide nucleating agent on the shear-induced crystallization behavior of isotactic polypropylene. *ACS. Appl. Polym. Mater.* **2021**, *3*, 1145–1156. [[CrossRef](#)]
6. Sowinski, P.; Piorkowska, E.; Boyer, S.A.E.; Haudin, J.M. High-pressure crystallization of iPP nucleated with 1, 3: 2, 4-bis (3, 4-dimethylbenzylidene) sorbitol. *Polymers* **2021**, *13*, 145. [[CrossRef](#)]
7. Murphy, I.A.; Rice, P.S.; Monahan, M.; Zasada, L.P.; Miller, E.M.; Rauegi, S.; Cossairt, B.M. Covalent functionalization of Nickel phosphide nanocrystals with aryl-diazonium salts. *Chem. Mater.* **2021**, *33*, 9652–9665. [[CrossRef](#)]
8. Zhang, Y.F. Comparison of nucleation effects of organic phosphorous and sorbitol derivative nucleating agents in isotactic polypropylene. *J. Macromol. Sci. B* **2008**, *47*, 1188–1196. [[CrossRef](#)]
9. Mohr, P.; Matic, A. Examination and experimental constraints of the stellar reaction rate factor N-A of the Ne-18(alpha, p)NA-21 reaction at temperatures of X-ray bursts. *Phys. Rev. C* **2013**, *87*, 035801. [[CrossRef](#)]
10. Mller, K.; Wienhfer, G.; Westerhaus, F.; Junge, K.; Beller, M. Oxidation of 1,2,4-trimethylbenzene (TMB), 2,3,6-trimethylphenol (TMP) and 2-methylnaphthalene to 2,3,5-trimethylbenzoquinone (TMBQ) and menadione (vitamin K3). *Catal. Today* **2011**, *173*, 68–75. [[CrossRef](#)]
11. Zhang, Y.F.; Zhong, X. Effects of substituted aromatic heterocyclic phosphate salts on properties, crystallization, and melting behaviors of isotactic polypropylene. *J. Appl. Polym. Sci.* **2010**, *100*, 4868–4874. [[CrossRef](#)]
12. Liu, Y.; Zhang, K.; Fu, G.; He, W.; Qin, S.; Yu, J. Synergistic effect of aryl heterocyclic aluminum phosphate and sodium laurate on non-isothermal crystallization kinetics of isotactic polypropylene. *J. Thermoplast. Compos.* **2017**, *30*, 678–690. [[CrossRef](#)]
13. Kimura, R.; Tuboi, T.; Nishikawa, K. Crystalline Synthetic Resin Composition. US Patent No 5,342,868, 30 August 1994.
14. Li, C.; Tong, C.; Meng, X.; Xin, Z.; Shi, Y. Effect of nucleating agent supported on zeolite via the impregnation on the crystallization ability of isotactic polypropylene and its mechanism. *Polym. Advan. Technol.* **2019**, *30*, 2674–2685. [[CrossRef](#)]
15. Liu, L.; Zhao, Y.; Zhang, C.; Dong, Z.; Wang, K.; Wang, D. Morphological characteristics of β -Nucleating agents governing the formation of the crystalline structure of isotactic Polypropylene. *Macromolecules* **2021**, *54*, 6824–6834. [[CrossRef](#)]
16. Thumm, A.; Risani, R.; Dickson, A.; Sorieul, M. Ligno-cellulosic fibre sized with nucleating agents promoting transcrystallinity in isotactic polypropylene composites. *Materials* **2020**, *13*, 1259. [[CrossRef](#)] [[PubMed](#)]
17. Long, L.; He, W.; Li, J.; Qin, S.; Yu, J. Nucleation ability of nonmetallic organophosphate derivatives in isotactic polypropylene. *J. Therm. Anal. Calorim.* **2017**, *127*, 2283–2291. [[CrossRef](#)]
18. Li, B.; Guo, H.H.; Gui, P.C.; Liu, T.; Zhao, L.; Yuan, W.K. Effect of supercritical carbon dioxide-assisted nano-scale dispersion of nucleating agents on the crystallization behavior and properties of polypropylene. *J. Supercrit. Fluid* **2008**, *44*, 446–456. [[CrossRef](#)]
19. Yang, B.; Wang, D.; Chen, F.; Su, L.F.; Miao, J.B.; Chen, P.; Liu, J.W. Melting and crystallization behaviors of poly (lactic acid) modified with graphene acting as a nucleating agent. *J. Macromol. Sci. B* **2019**, *58*, 290–304. [[CrossRef](#)]
20. Gao, J.; Meng, X.; Deng, Z.; Xin, Z.; Tong, C. Enhancement of “in-situ” dispersed NA11 for the mechanical and crystallization properties of polypropylene. *J. Polym. Res.* **2022**, *29*, 168.
21. Meng, X.; Tong, C.; Xin, Z.; Gong, W.; Shi, Y.; Chen, W.; Sheng, Y. Promotion of zeolite as dispersion support for properties improvement of α nucleating agent in polypropylene. *J. Polym. Res.* **2019**, *26*, 105. [[CrossRef](#)]
22. Yue, Y.; Yi, J.; Wang, L.; Feng, J. Toward a more comprehensive understanding on the structure evolution and assembly formation of a bisamide nucleating agent in polypropylene melt. *Macromolecules* **2020**, *53*, 4381–4394. [[CrossRef](#)]
23. Zhang, G.P.; Xin, Z.; Yu, J.Y.; Gui, Q.D.; Wang, S.Y. Nucleating efficiency of organic phosphates in polypropylene. *J. Macromol. Sci. B* **2003**, *42*, 467–478. [[CrossRef](#)]

24. Long, L.; He, W.; Zhang, M.; Zhang, K.; Qin, S.; Yu, J. Nucleation effects of sodium and ammonium salts of 2,2'-methylene-bis-(4,6-di-*t*-butylphenylene)phosphate in isotactic polypropylene. *Polym. Eng. Sci.* **2015**, *55*, 22–28. [[CrossRef](#)]
25. Gabrielli, S.; Pastore, G.; Stella, F.; Marcantoni, E.; Sarasini, F.; Tirillò, J.; Santulli, C. Chemical and mechanical characterization of licorice root and palm leaf waste incorporated into Poly (urethane-acrylate)(PUA). *Molecules* **2021**, *26*, 7682. [[CrossRef](#)]
26. Mahmood, A.; Wang, X.; Xie, X.; Sun, J. Degradation behavior of mixed and isolated aromatic ring containing VOCs: Langmuir-Hinshelwood kinetics, photodegradation, in-situ FTIR and DFT studies. *J. Environ. Chem. Eng.* **2021**, *9*, 105069. [[CrossRef](#)]
27. Huang, W.J.; He, W.T.; Yu, J.; Zhang, K.; Qin, S.H.; Gao, J. Synthesis, characterization and application of 2, 2'-methylene-bis (4,6-di-*tert*-butyl-phenyl) phosphate sodium. In *Advanced Materials Research*; Trans Tech Publications Ltd.: Bäch, Switzerland, 2014; Volume 834, pp. 119–123.
28. ElOkr, M.M.; Metawe, F.; El-Nahrawy, A.M.; Osman, B.A. Enhanced structural and spectroscopic properties of phosphosilicate nanostructures by doping with Al₂O₃ ions and calcinations temperature. *Int. J. Chem. Tech. Res.* **2016**, *9*, 228–234.
29. Krivdin, L.B. Computational 1H NMR: Part 2. Chemical applications. *Magn. Reson. Chem.* **2020**, *58*, 5–14. [[CrossRef](#)]
30. Tang, Q.; Gao, K. Structure analysis of polyether-based thermoplastic polyurethane elastomers by FTIR, 1H NMR and 13C NMR. *Int. J. Polym. Anal. Charact.* **2017**, *22*, 569–574. [[CrossRef](#)]
31. Wang, Q.; Cui, D.; Wang, P.; Bai, J.; Wang, Z.; Liu, B. A comparison of the structures of >300 °C fractions in six Chinese shale oils obtained from different locations using 1H NMR, 13C NMR and FT-IR analyses. *Fuel* **2018**, *211*, 341–352. [[CrossRef](#)]
32. Srivastava, A.; Mishra, R.; Kumar, S.; Dev, K.; Tandon, P.; Maurya, R. Molecular structure, spectral investigation (1H NMR, 13C NMR, UV-Visible, FT-IR, FT-Raman), NBO, intramolecular hydrogen bonding, chemical reactivity and first hyperpolarizability analysis of formononetin [7-hydroxy-3 (4-methoxyphenyl) chromone]: A quantum chemical study. *J. Mol. Struct.* **2015**, *1084*, 55–73.
33. Barczewski, M.; Mysiukiewicz, O.; Matykiewicz, D.; Skórczewska, K.; Lewandowski, K.; Andrzejewski, J.; Piasecki, A. Development of polylactide composites with improved thermomechanical properties by simultaneous use of basalt powder and a nucleating agent. *Polym. Compos.* **2020**, *41*, 2947–2957. [[CrossRef](#)]
34. Xu, F.; Wang, B.; Yang, D.; Hao, J.; Qiao, Y.; Tian, Y. Thermal degradation of typical plastics under high heating rate conditions by TG-FTIR: Pyrolysis behaviors and kinetic analysis. *Energy Convers. Manag.* **2018**, *171*, 1106–1115. [[CrossRef](#)]
35. Yao, J.; Luo, F.; Mao, J.; Li, Y.; Sun, X.; Ma, D.; Li, L. Effects of crystal planes of ZnO nanocrystal on crystalline, thermal and thermal-oxidation stability of iPP. *J. Polym. Res.* **2021**, *28*, 172. [[CrossRef](#)]
36. He, M.; Shi, H.; Chang, B.; Zheng, G.; Cao, W.; Liu, C.; Shen, C. The synergistic effect of rare-earth complex nucleating agent and graphene oxide on the non-isothermal crystallization behavior of iPP originating from the diverse self-assembly morphology. *Macromol. Chem. Phys.* **2021**, *222*, 2000357. [[CrossRef](#)]
37. Zhang, Y.F.; He, B.; Hou, H.H.; Guo, L.H. Isothermal crystallization of isotactic polypropylene nucleated with a novel aromatic heterocyclic phosphate nucleating agent. *J. Macromol. Sci. B* **2017**, *56*, 811–820. [[CrossRef](#)]
38. Shi, W.; Xu, Y.; Qin, J.; Li, X.; Lv, Q.; Chen, X.; Chen, M. Isothermal crystallization behaviors of isotactic polypropylene with ultrasonically-modified calcium sulfate whisker as β -nucleating agent. *Polym. Eng. Sci.* **2022**, *62*, 2219–2229. [[CrossRef](#)]
39. Fang, W.; Yang, X.; Xu, X.; Li, W.; Li, Q. Quasi-static and low-velocity impact responses of polypropylene random copolymer composites with adjustable crystalline structures. *Compos. Part. B Eng.* **2021**, *224*, 109139. [[CrossRef](#)]
40. Rasana, N.; Jayanarayanan, K.; Pegoretti, A. Non-isothermal crystallization kinetics of polypropylene/short glass fibre/multiwalled carbon nanotube composites. *RSC Adv.* **2018**, *8*, 39127–39139. [[CrossRef](#)]
41. Mao, J.J.; Jiang, Y.Z.; Zhou, P.Z.; Li, Y.; Zhang, Y.F. Nucleus density and crystallization behavior of isotactic polypropylene nucleated with different α/β compound nucleating agents. *J. Therm. Anal. Calorim.* **2020**, *140*, 2275–2282. [[CrossRef](#)]
42. Wang, Y.J.; Yan, S.Y.; Zhao, Z.P.; Xi, Z.Y. Isothermal crystallization of iPP in environment-friendly diluents: Effect of binary diluents and crystallization temperature on crystallization kinetics. *Chin. J. Polym. Sci.* **2019**, *37*, 617–626. [[CrossRef](#)]
43. Suksut, B.; Saiprasit, P.; Schlarb, A.K. Isothermal crystallization of polypropylene/titanium dioxide nanocomposites by flash scanning calorimetry. *Asia-Pac. J. Sci. Technol.* **2021**, *26*, 1–7.
44. Shang, Y.; Ning, P.; Zhang, Y.; Xue, F.; Cai, Z.; Li, J.; Jiang, S. Study on structure and property relations of α -iPP during uniaxial deformation via in situ synchrotron SAXS/WAXS and POM investigations. *Polym. Eng. Sci.* **2018**, *58*, 160–169. [[CrossRef](#)]
45. Cavicchi, K.A.; Pantoja, M.; Lai, T.Y. The importance of phase behavior in understanding structure-property relationships in crystalline small molecule/polymer gels. In *Gels and Other Soft Amorphous Solids*; American Chemical Society: Washington, DC, USA, 2018; pp. 245–264.
46. McCreath, S.; Boinard, P.; Boinard, E.; Gritter, P.; Liggat, J.J. High clarity polyurethane laminating adhesives based on poly(propylene glycol). Effect of hard segment on microphase morphology, haze and adhesion. *Int. J. Adhes. Adhes.* **2022**, *117*, 103168. [[CrossRef](#)]
47. Long, Y.; Wang, Y.; Xing, Q.; Dong, X. Enhanced crystallization behavior and stiffness-toughness balance of polylactide/poly(propylene carbonate)/nucleating agent blends. *Thermochim. Acta* **2022**, *711*, 179207. [[CrossRef](#)]